Physical model study of orthorhombic anistotropy

S. P. Cheadle and D. C. Lawton

ABSTRACT

An industrial laminate is shown to possess elastic anisotropy. The material, Phenolic CE, is composed of thin layers of canvas fabric bonded with a phenolic resin. Ultrasonic physical modeling has been conducted using the phenolic. Different compressional-wave velocities and distinct patterns of shear-wave splitting are observed on each face of a cube of the material, as well on edges of the cube beveled at 45° to the adjacent faces. Analysis of the results demonstrate that the phenolic laminate is suitable for modeling media with anisotropy of orthorhombic symmetry.

INTRODUCTION

Shear-wave splitting and anisotropy are being studied as part of the ongoing effort to enhance seismic data interpretation and reservoir exploitation. Multicomponent surface seismic, VSP, crosswell and full waveform sonic data are being used to determine the relationship between shear mode polarization and fracture patterns (Crampin, 1981, 1984, 1985; Yale and Sprunt, 1989). Banik (1984) reported errors in depth estimates of between 150 - 300 m in areas of the North Sea basin due to anisotropy within some shaly units. Both compressional and shear wave anisotropy impact on velocity analysis for multicomponent imaging and methods of estimating stress based on the Vs/Vp ratio (Thomsen, 1986, 1988). To address these issues, a clearer understanding of elastic wave propagation in anisotropic media is required.

Numerical and physical modeling can be used to study shear-wave splitting and anisotropy. Numerical techniques are useful for estimating the response of specific cases for an approximated or well understood system. Physical modeling is useful for studying complex or poorly understood systems, such as anisotropic media. This paper describes the results of experiments to determine the anisotropic elastic properties of an industrial laminate, Phenolic CE. Velocity measurments and observations of shear-wave splitting at various directions through a cube of the phenolic are interpreted in terms of orthorhombic anisotropy.

PHYSICAL MODEL EXPERIMENTS

Physical modeling generates data that are being used to test multicomponent processing and numerical modeling techniques under development as part of the Consortium for Research in Elastic Wave Exploration Seismology (CREWES) project at the University of Calgary. Ultrasonic modeling using phenolic laminate is ideally suited to study velocity anisotropy because the ambiguities inherent in field data are absent. The initial effort has been to determine the anisotropic behaviour of phenolic for compressional and shear waves.

Piezoelectric P-wave and S-wave transducers are being used as the acoustic source and receivers for multicomponent physical modeling. Both are flat-faced cylindrical contact transducers with an active element 1.26 cm in diameter. The compressional or P-wave

transducer (Panametrics V103) is vertically polarized, with the maximum sensitivity normal to the contact face. The shear-wave transducer (Panametrics V153) is horizontally polarized, with the maximum sensitivity parallel to a line across the contact face. To record the SV or radial component, the shear receiver transducer is used with the polarization parallel to the spread direction, while for the SH or transverse component, the receiver is rotated with the polarization perpendicular to the azimuth of the profile plane.

The source transducer is driven with a 28-volt square wave tuned to produce a broadband wavelet with a centre frequency at 600 kHz. Amplified data are sampled and stored using a Nicolet digital recording oscilloscope, connected to a Perkin-Elmer 3220 seismic processing system through an IBM-XT which controls the experiments. Traces of up to 4096 samples are recorded sequentially and stored on tape or disc in standard SEG-Y format.

The CE grade phenolic laminate is composed of layers of a woven canvas fabric saturated and bonded with a phenolic resin, and has a density of 1360 kg/m^3. Other grades of laminate which incorporate thin paper layers, fibre glass cloth or linen are also available. Initial tests with the phenolic used in this study showed that there was a directional dependancy on the velocity for both P and S waves, suggesting it was suitable for a modeling study of an anisotropic medium. Shear-wave splitting was observed during transmission tests when the sample was rotated between shear transducers with parallel polarization. The polarizations of the split shear waves also appeared to be parallel to the orientations of the approximately orthogonal weave of fibres in the canvas fabric. For this reason, subsequent experiments were conducted on pieces of phenolic that were cut with faces parallel or orthogonal to the observed fibre directions and to the plane of the canvas layers.

SHEAR-WAVE SPLITTING

Shear-wave splitting experiments were conducted using a 10 cm. cube of phenolic. A sample of the CE grade phenolic with the faces labeled with the convention used in this study is shown in Figure 1. The machined surface of the laminate sheet, parallel to the fabric layers, was designated Face 1, while the sides of the cube, parallel to the fibre directions, were designated Faces 2 and 3. The apparatus used for studying split shear waves is shown in Figure 2. The cube of material is placed between two fixed shear wave transducers which are aligned with parallel polarizations. The cube can rotate between the transducers, and a pointer on the cube is used to determine the azimuth of the sample with respect to a fixed circular protractor.

Figures 3, 4 and 5 show the records form Faces 1, 2 and 3 of the cube respectively. Each trace records the signal transmitted through the cube at 5° intervals of rotation with respect to the polarization direction of the shear-wave transducers. The sample rate used in this study was 50 nanoseconds, and the arrival times are shown in microseconds. The arrival times and hence the velocities of the two shear components do not vary with azimuth on a particular face. The faster shear arrival is designated S_1 and the slower mode as S_2. While it is stictly correct to refer to the split shear waves and the P waves under most conditions as quasishear and quasicompressional modes, that prefix will be implied rather than included. On all records, the weakly coupled P-wave arrival is barely visible. The compressional velocities were determined separately using the P-wave transducers.

The orthogonal relationship between the fast and slow shear modes is clearly observed as the 90° separation of the amplitude maxima of the split shear arrivals. An example of a plot of amplitude vs. azimuth for a record from Face 2 is shown in Figure 6. Figure 3, plotted in true relative amplitude, and Figure 6 both show that the S_1 mode generally has a greater amplitude than the S_2 arrival, indicating that the attenuation is also dependent on the polarization of particle motion. The amplitude ratios of the fast to slow

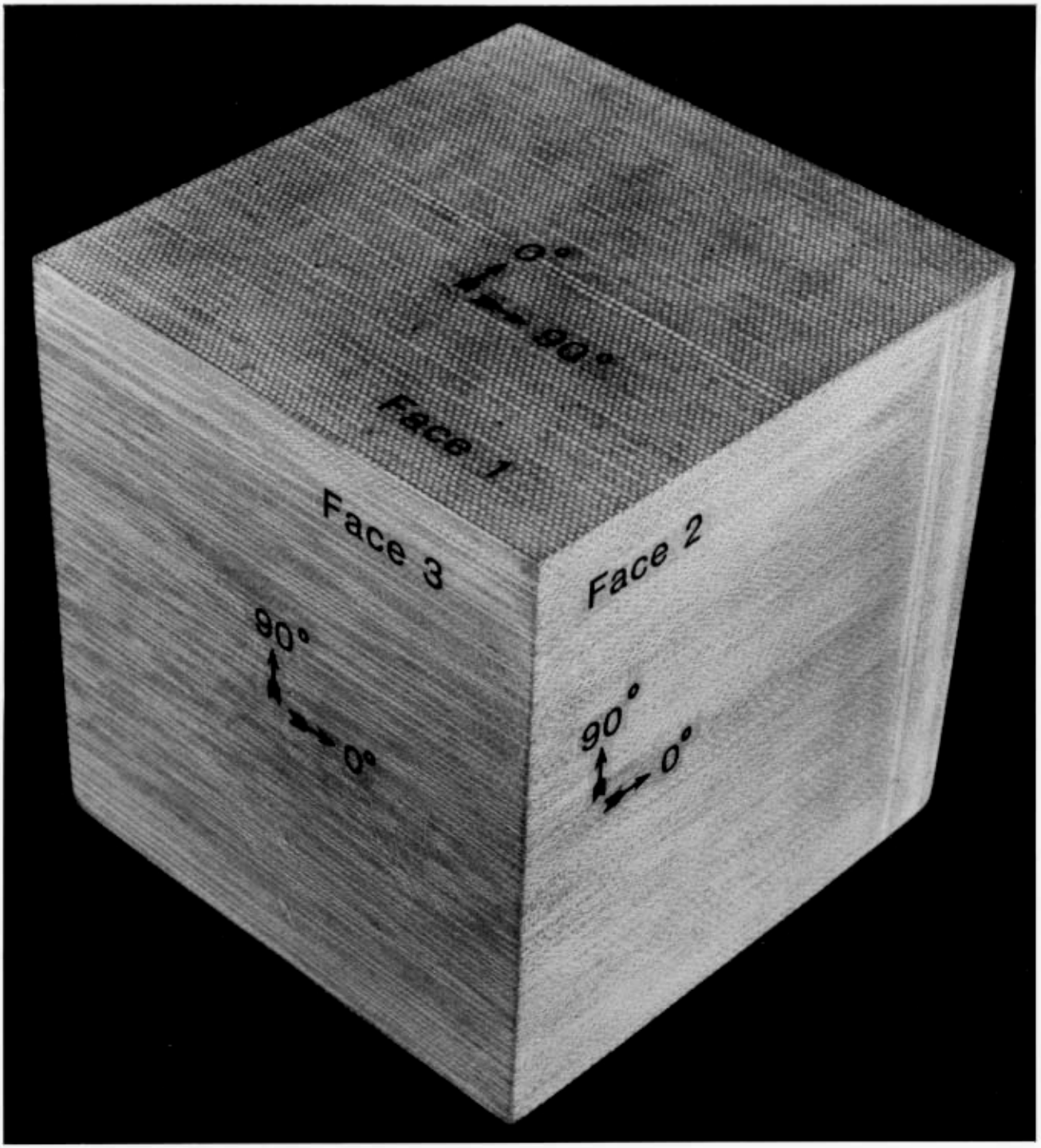

FIG. 1. Phenolic CE laminate is composed of layers of a canvas weave fabric bonded with phenolic resin. The faces are labeled as used in this study.

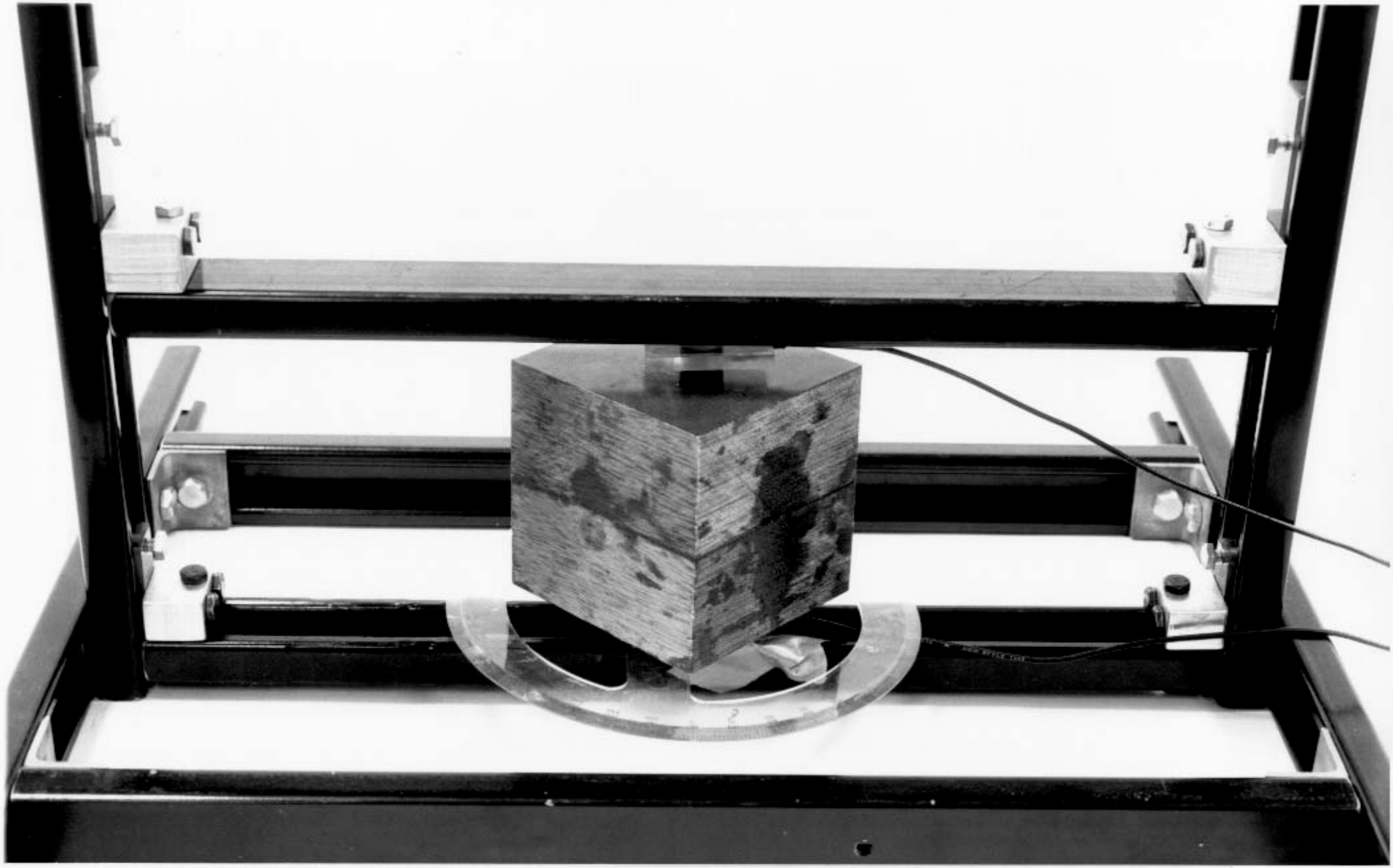

FIG. 2. The apparatus used for shear-wave splitting experiments clamps the cube of phenolic between two shear-wave transducers of parallel polarization. The cube is rotated while the transducers remain fixed. A circular protractor scale is used to determine the azimuth of the rotation.

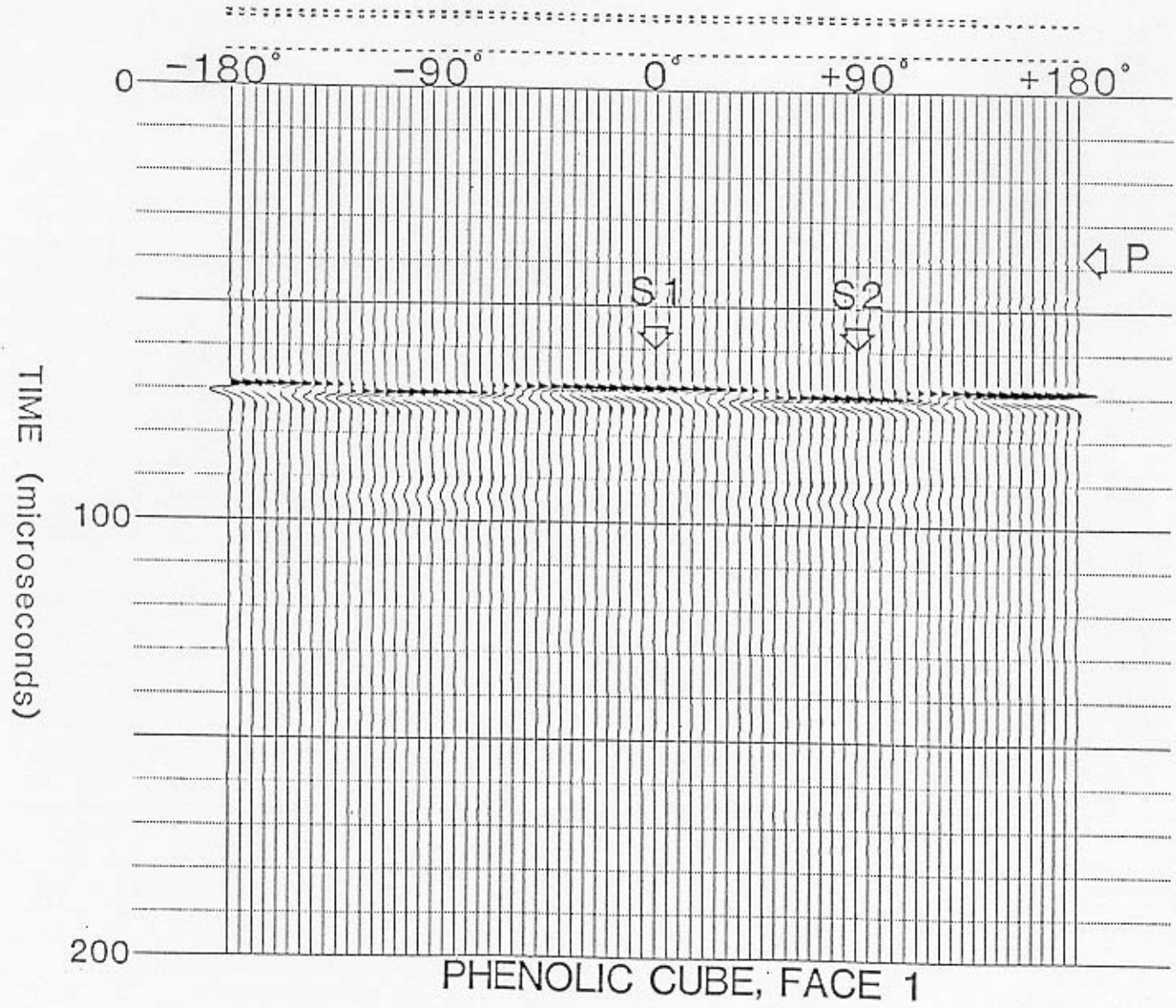

FIG. 3. The record from Face 1 of the 10 cm. cube of phenolic laminate showing the orthogonal relationship between the amplitude maxima of the faster S1 (1608 m/s) and slower S2 (1520 m/s) shear waves. The compressional velocity through Face 1, determined separately with P-wave transducers, is 2927 m/s. The traces were recorded at 5° intervals of rotation.

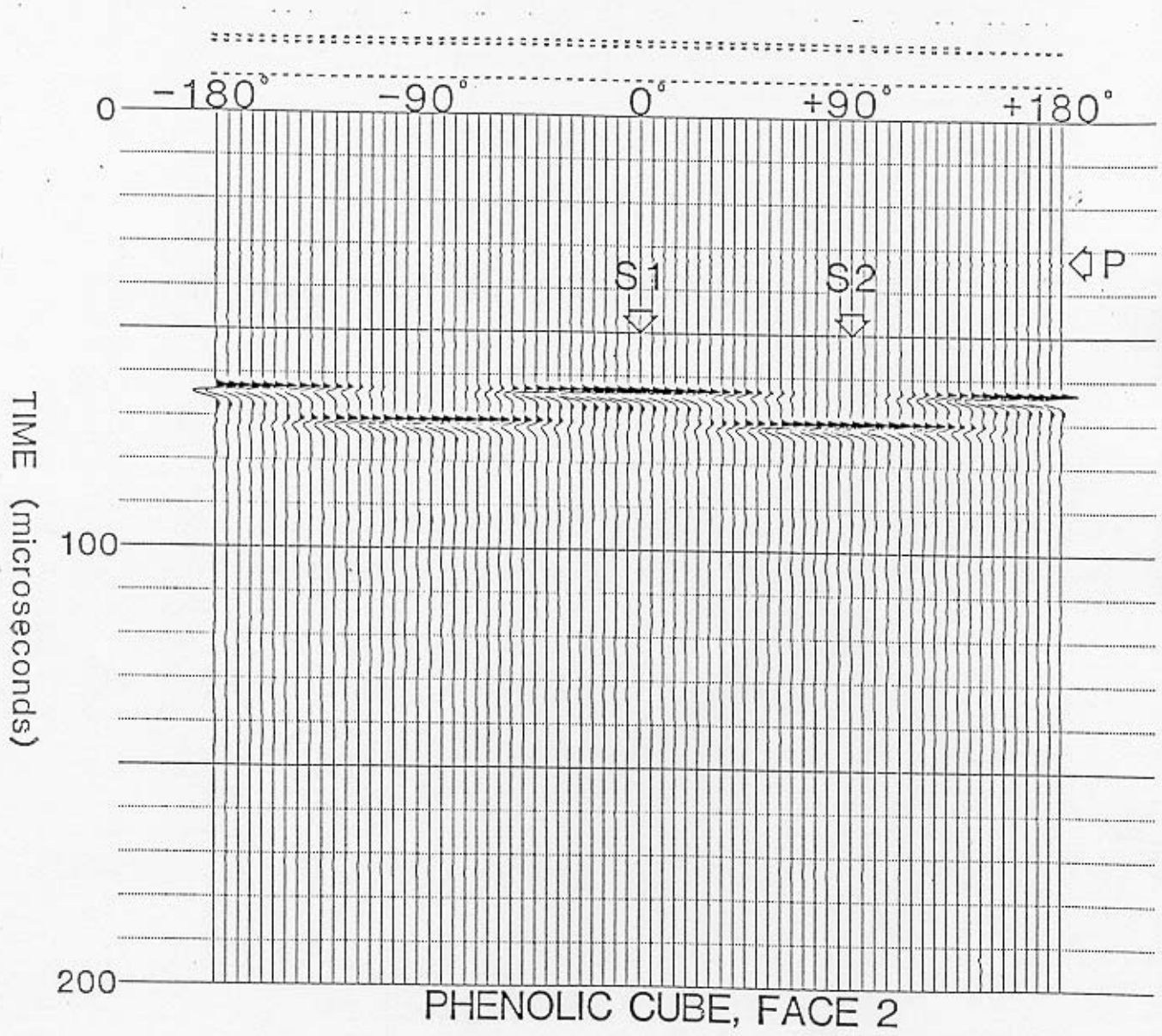

FIG. 4. The record from Face 2, showing the faster S1 arrival at 1656 m/s and the slower S2 arrival at 1504 m/s. The compressional velocity through Face 2 is 3376 m/s.

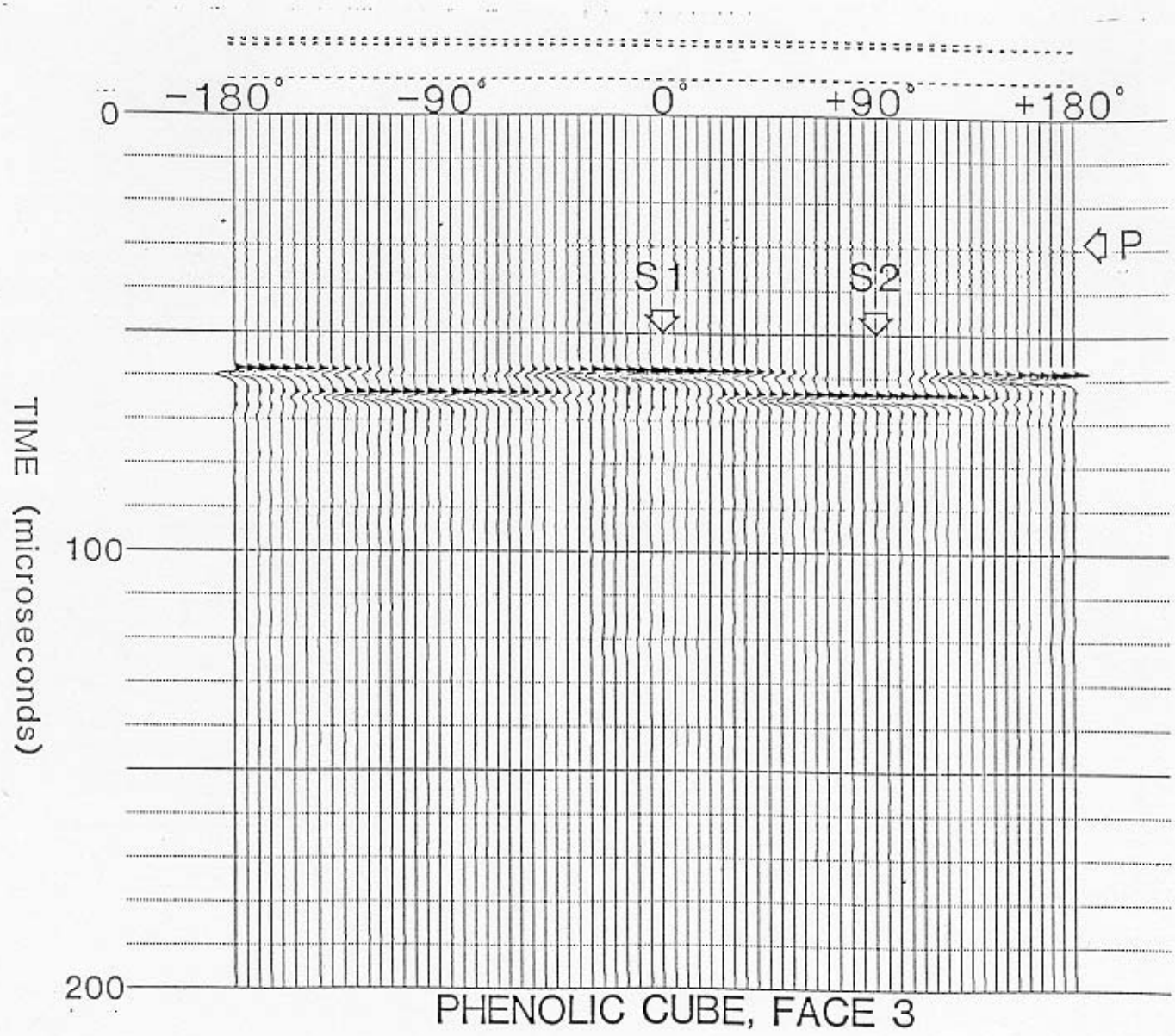

FIG. 5. The record from Face 3, showing the faster S1 arrival at 1663 m/s and the slower S2 arrival at 1597 m/s. The compressional velocity through Face 3 is 3575 m/s.

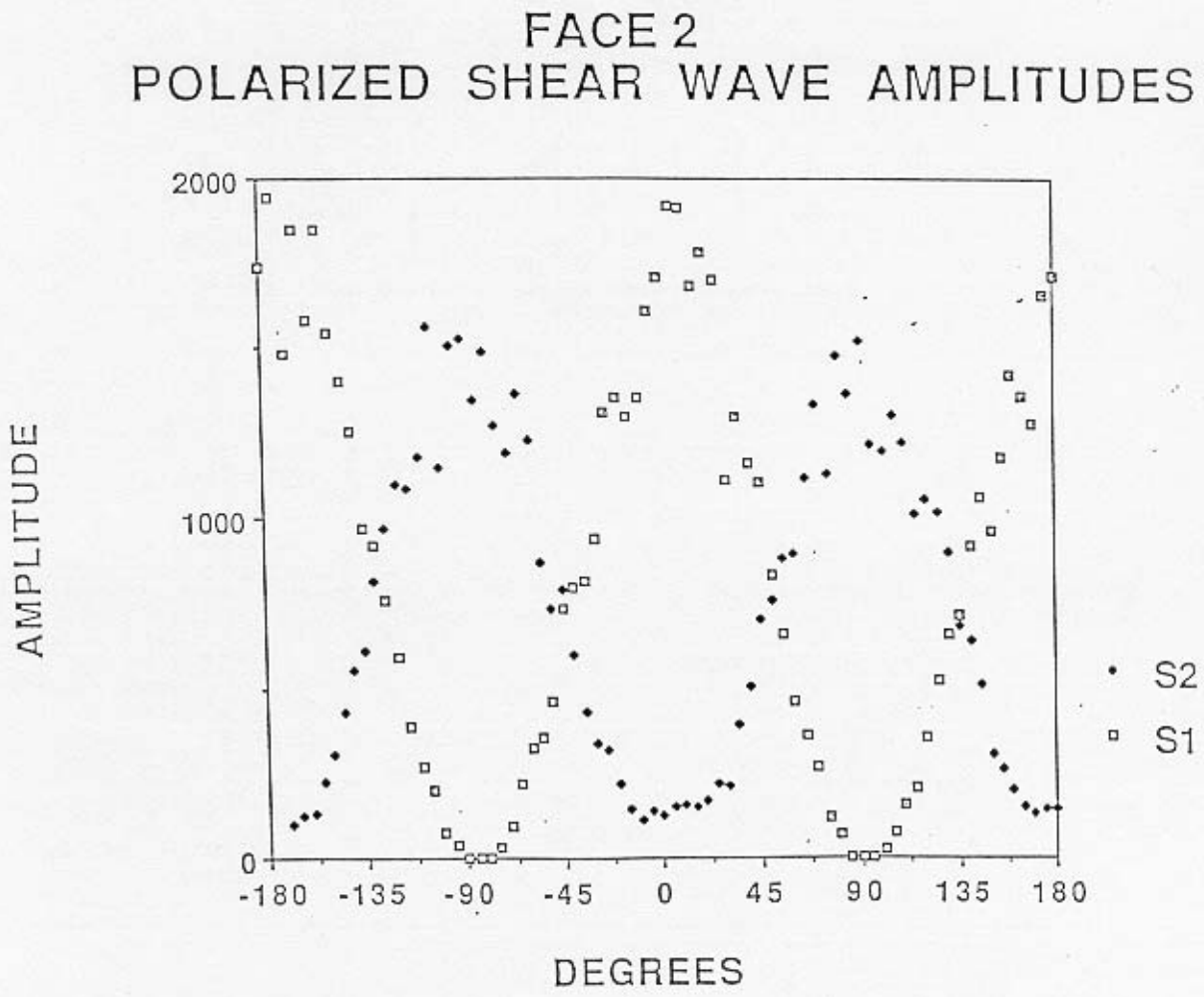

FIG. 6. The amplitude vs. azimuth of the sample with respect to the polarization direction of the shear-wave transducers for a record from Face 2. The scatter of the measured amplitudes is related to the coupling of the transducers.

shear arrivals, measured at their maxima, have varied from 1.1/1.0 to 1.4/1.0 for the samples tested.

The P, S_1 and S_2 velocities measured on each face are summarized in Figure 7. For the following discussion, the velocities will be labelled with 2 subscripts indicating the directions of propagation and particle motion with respect to the three faces of the cube. For example, V_{12} indicates wavefield propagation through Face 1 with particle motion towards Face 2. Slow, medium and fast directions through the cube may be defined on the basis of the measured compressional velocities, ie. V_{11} = 2927 m/s, V_{22} = 3376 m/s and V_{33} = 3575 m/s respectively. Of the six shear wave velocities measured there are only three independent values, which depend on the direction of propagation and particle motion. The shear wave velocities may be paired as follows;

1) propagation in the medium direction and particle motion in the slow direction, or vice versa (V_{21} = 1504 m/s, V_{12} = 1520 m/s),

2) propagation in the fast direction and particle motion in the slow direction, or vice versa (V_{31} = 1597 m/s, V_{13} = 1608 m/s),

3) propagation in the medium direction and particle motion in the fast direction, or vice versa (V_{23} = 1656 m/s, V_{32} = 1663 m/s).

Transmission experiments were also performed between opposing edges of the cube after they were beveled at 45° to the adjacent faces. The measured P, S_1 and S_2 velocities are summarized on Figure 8. Transmission in the 2-3 plane perpendicular to the axis through Face 1 will be designated as the 4 direction, with V_{44} referring to the P-wave, V_{44}^{-} referring to the SV mode in the 2-3 plane and V_{41} referring to the SH mode with particle motion towards Face 1. Similarly, the 5 direction is in the 1-3 plane perpendicular to the axis through Face 2 and the 6 direction is in the 1-2 plane perpendicular to the axis through Face 3.

The measured velocities for a particular sample of phenolic are repeatable to within +/- 15 m/s (~0.5%) for P-waves and +/- 4 m/s (~0.25%) for shear waves, corresponding to +/- 3 time points at the sample rate that was used. Variations between different samples were approximately twice that again. Based on visual inspection, there is some spatial variation in the fibre density within a sheet that may cause the velocity differences observed. The velocity values are based on transit time measurements of the start of the wavelet, with a small delay time related to the transducer response subtracted.

ORTHORHOMBIC ANISOTROPY

The results of the transmission experiments with the phenolic indicate that the orthorhombic symmetry system is appropriate to describe the anisotropy of this material. Following the indicial notation used by Thomsen (1986), stress σ and strain E are related by

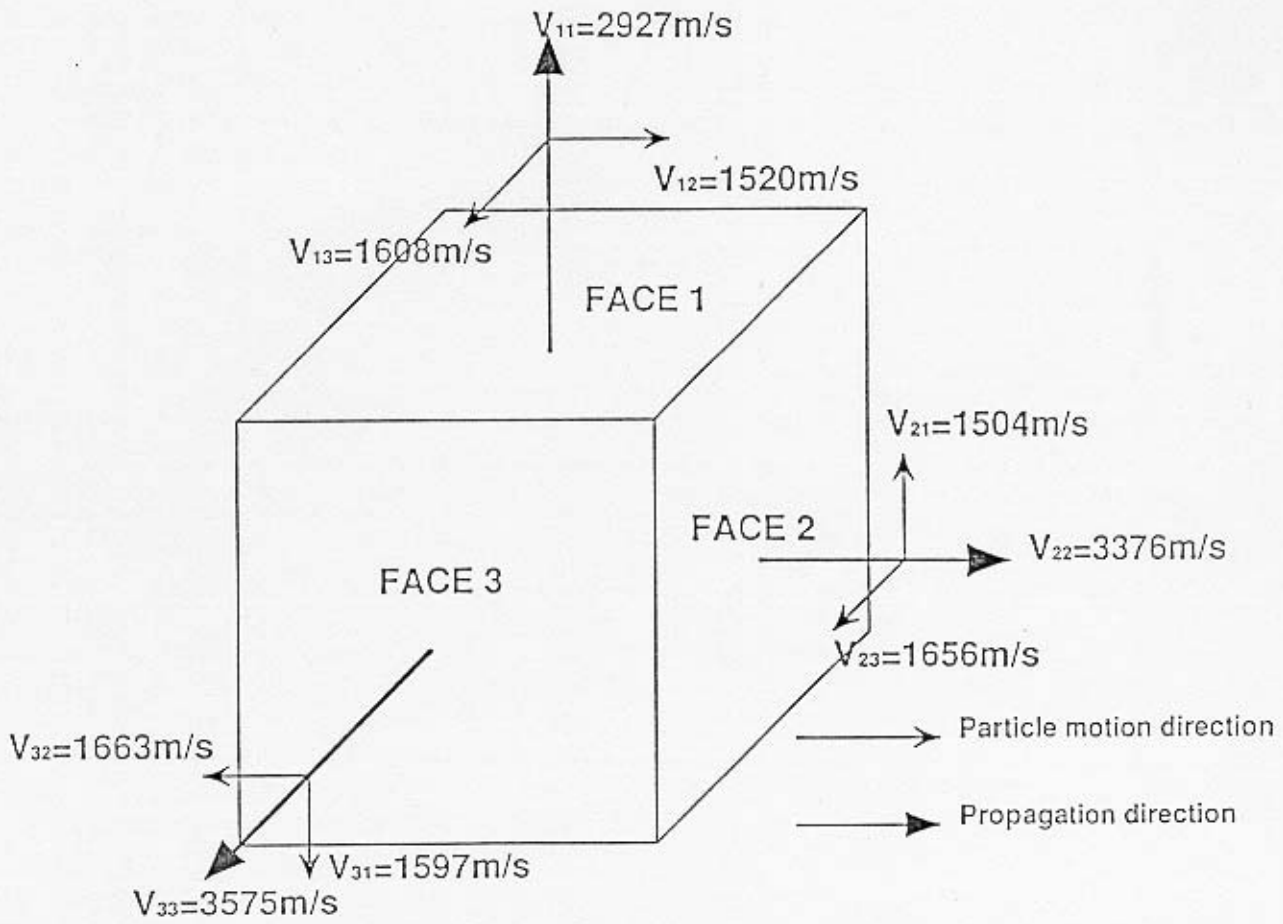

FIG. 7. The measured P-wave and S-wave velocities measured along the principal axes are summarized, with the heavy arrow designating the direction of propagation and the lighter arrow the direction of particle motion of the shear waves. The subscripts correspond to the directions of propagation and particle motion respectively. Of the six shear wave velocities, three distinct pairs of values are recognized.

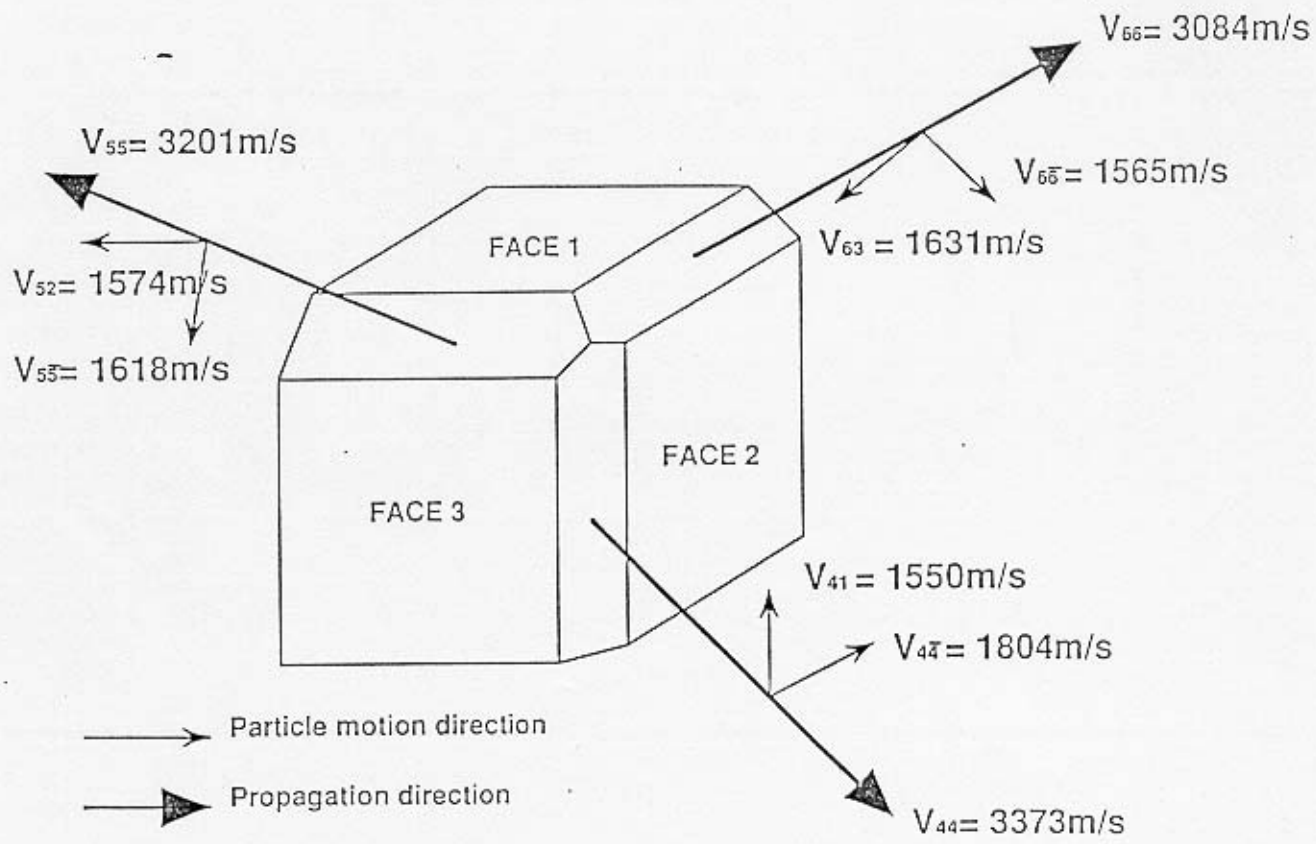

FIG. 8. The results of transmission measurements between opposing edges of the phenolic cube are summarized. The propagation directions were at 45° to two of the principal axes and perpendicular to the third.

$$\sigma_{ij} = \sum_{k=1}^{3} \sum_{1=1}^{3} c_{ijkl}\varepsilon_{kl} , \qquad i, j, = 1, 2, 3 \qquad 1)$$

For the case of orthorhombic symmetry, the 3x3x3x3 stiffness tensor c_{ijkl} may be reduced to a 6x6 matrix

$$c_{mn} = \begin{bmatrix} c_{11} & c_{12} & c_{13} & & & \\ & c_{22} & c_{23} & & & \\ & & c_{33} & & & \\ & & & c_{44} & & \\ & & & & c_{55} & \\ & & & & & c_{66} \end{bmatrix} \qquad (2)$$

of nine independent coefficients, with $c_{12} = c_{21}$, $c_{13} = c_{31}$, and $c_{23} = c_{32}$ (Nye, 1957; Fedrov, 1968; Musgrave, 1970). Using the elastic equation of motion Brown, 1989; in this volume) acoustic velocities may be defined in terms of the stiffnesses c_{mn} and the density ρ as follows; Along the principal axes,

$$V_{11} = \sqrt{(c_{11}/\rho)}, \qquad (3)$$

$$V_{22} = \sqrt{(c_{22}/\rho)}, \qquad (4)$$

$$V_{33} = \sqrt{(c_{33}/\rho)}, \qquad (5)$$

$$V_{23} = V_{32}\sqrt{(c_{44}/\rho)}, \qquad (6)$$

$$V_{13} = V_{31}\sqrt{(c_{55}/\rho)}, \qquad (7)$$

$$V_{12} = V_{21}\sqrt{(c_{66}/\rho)}, \qquad (8)$$

For a raypath in the 2-3 plane at 45° to those principal axes and perpendicular to the axis through Face 1,

$$V_{44} = \sqrt{\left[\left\{(c_{22} + c_{33} + 2c_{44}) + \left[(c_{33} - c_{22})^2 + 4(c_{23} + c_{44})^2\right]^{1/2}\right\}/4\rho\right]} \quad (9)$$

$$V_{4\bar{4}} = \sqrt{\left[\left\{(c_{22} + c_{33} + 2c_{44}) - \left[(c_{33} - c_{22})^2 + 4(c_{23} + c_{44})^2\right]^{1/2}\right\}/4\rho\right]} \quad (10)$$

$$V_{41} = \sqrt{\left[(c_{55} + c_{66})/2\rho\right]} \quad (11)$$

Similarly, for a raypath in the 1-3 plane at 45° to those axes and perpendicular to the axis through Face 2,

$$V_{55} = \sqrt{\left[\left\{(c_{11} + c_{33} + 2c_{55}) + \left[(c_{11} - c_{33})^2 + 4(c_{13} + c_{66})^2\right]^{1/2}\right\}/4\rho\right]} \quad (12)$$

$$V_{5\bar{5}} = \sqrt{\left[\left\{(c_{11} + c_{33} + 2c_{55}) - \left[(c_{11} - c_{33})^2 + 4(c_{13} + c_{66})^2\right]^{1/2}\right\}/4\rho\right]} \quad (13)$$

$$V_{52} = \sqrt{\left[(c_{44} + c_{66})/2\rho\right]} \quad (14)$$

and for a raypath in the 1-2 plane at 45° to those axes and perpendicular to the axis through Face 3,

$$V_{66} = \sqrt{\left[\left\{(c_{11} + c_{22} + 2c_{66}) + \left[(c_{22} - c_{11})^2 + 4(c_{12} + c_{66})^2\right]^{1/2}\right\}/4\rho\right]} \quad (15)$$

$$V_{6\bar{6}} = \sqrt{\left[\left\{(c_{11} + c_{22} + 2c_{66}) - \left[(c_{22} - c_{11})^2 + 4(c_{12} + c_{66})^2\right]^{1/2}\right\}/4\rho\right]} \quad (16)$$

$$V_{63} = \sqrt{\left[(c_{44} + c_{55})/2\rho\right]} \quad (17)$$

Nine independent velocity values are required to completely define the stiffnesss matrix for the case of orthorhombic anisotropy. These include the three P wave velocities along the principal axes, three shear wave velocities, one of each pair, also along the principal axes, and three P wave or SV wave velocities, each perpendicular to one and at 45° to the other two principal axes. In principal, measurements at other orientations could be used but require considerably more complex solutions.

Using the relationships outlined above, the measured velocities can be used to calculate the stiffness coefficients and to determine how well the data from the Phenolic CE corresponds to the model of orthorhombic anisotropy. Firstly, it is required that $V_{12} = V_{21}$, $V_{13} = V_{31}$ and $V_{23} = V_{32}$. From Figure 6, this can be seen to be the case, with differences of 1% or less. The stiffness coefficients determined from the shear velocities along the principal axes, ie. c_{44}, c_{55} and c_{66} can be used to calculate the SH mode velocities along the 45° raypaths using Equations 11, 14 and 17. The stiffness coefficients off the diagonal of the matrix, ie. c_{12}, c_{13} and c_{23}, can be computed using either the P-wave or the SV-wave velocities from the 45° raypaths. For example, either V_{44} or $V_{4\bar{4}}$ can be used in the computation of a value for c_{23}. Separate stiffnesses were computed using the measured P-wave and SV-wave velocities, and then the average of the two coefficients was used to compute the corresponding model velocities. The results are summarized in Table 1.

The measured velocities fit the orthorhombic symmetry model very well, with the largest deviations noted for the SV modes in the 5 and 6 directions. No explanation has been determined for the consistency of the negative bias in the differences between the measured and model velocities. However, the results indicate that the phenolic is suitable for physical modeling of orthorhombic anisotropy.

DISCUSSION

The source of the anisotropy in the phenolic laminate appears to be related to the layering and weave of the canvas fabric, with different fibre densities in the directions of the three principal axes. Thin sections cut parallel to the three faces of the phenolic cube are shown in Figure 9. The causes of anisotropy in natural rocks include thin layer lamination (Helbig, 1983) and preferred orientation of mineral grains, pores or fractures (Crampin, 1985). Anisotropy has been recognized in many rocks (Thomsen, 1986; Banik, 1984), but the physical cause and symmetry systems of specific cases of anisotropic media are seldom unambiguously identified. Transverse isotropy can be invoked for thin bed layering or

Table 1. The stiffness coefficient matrix and the comparison of the measured vs. computed velocities.

c_{11} = 11.65157 x 10^9 N/m^2
c_{22} = 15.50043 "
c_{33} = 17.38165 "
c_{44} = 3.747616 "
c_{55} = 3.494668 "
c_{66} = 3.109156 "
c_{23} = 7.259130 (average from V_{44} and $V_{4\bar{4}}$)
(6.968318 from V_{44}, 7.549941 from $V_{4\bar{4}}$)

c_{13} = 6.475514 (average from V_{55} and $V_{5\bar{5}}$)
(5.938791 from V_{55}, 7.012237 from $V_{5\bar{5}}$)

c_{12} = 6.299762 (average from V_{66} and $V_{6\bar{6}}$)
(5.871894 from V_{66}, 6.727631 from $V_{6\bar{6}}$)

Computed velocity	Measured velocity	Error
v_{44} = 3389 m/s,	v_{44} = 3373 m/s	-0.5%
$v_{4\bar{4}}$ = 1833 m/s	$v_{4\bar{4}}$ = 1804 m/s	-1.6%
v_{41} = 1558 m/s	v_{41} = 1550 m/s	-0.5%
v_{55} = 3230 m/s	v_{55} = 3201 m/s	-0.9%
$v_{5\bar{5}}$ = 1676 m/s	$v_{5\bar{5}}$ = 1618 m/s	-3.5%
v_{52} = 1588 m/s	v_{52} = 1574 m/s	-0.9%
v_{66} = 3109 m/s	v_{66} = 3084 m/s	-0.8%
$v_{6\bar{6}}$ = 1613 m/s	$v_{6\bar{6}}$ = 1565 m/s	-3.0%
v_{63} = 1632 m/s	v_{63} = 1631 m/s	0%

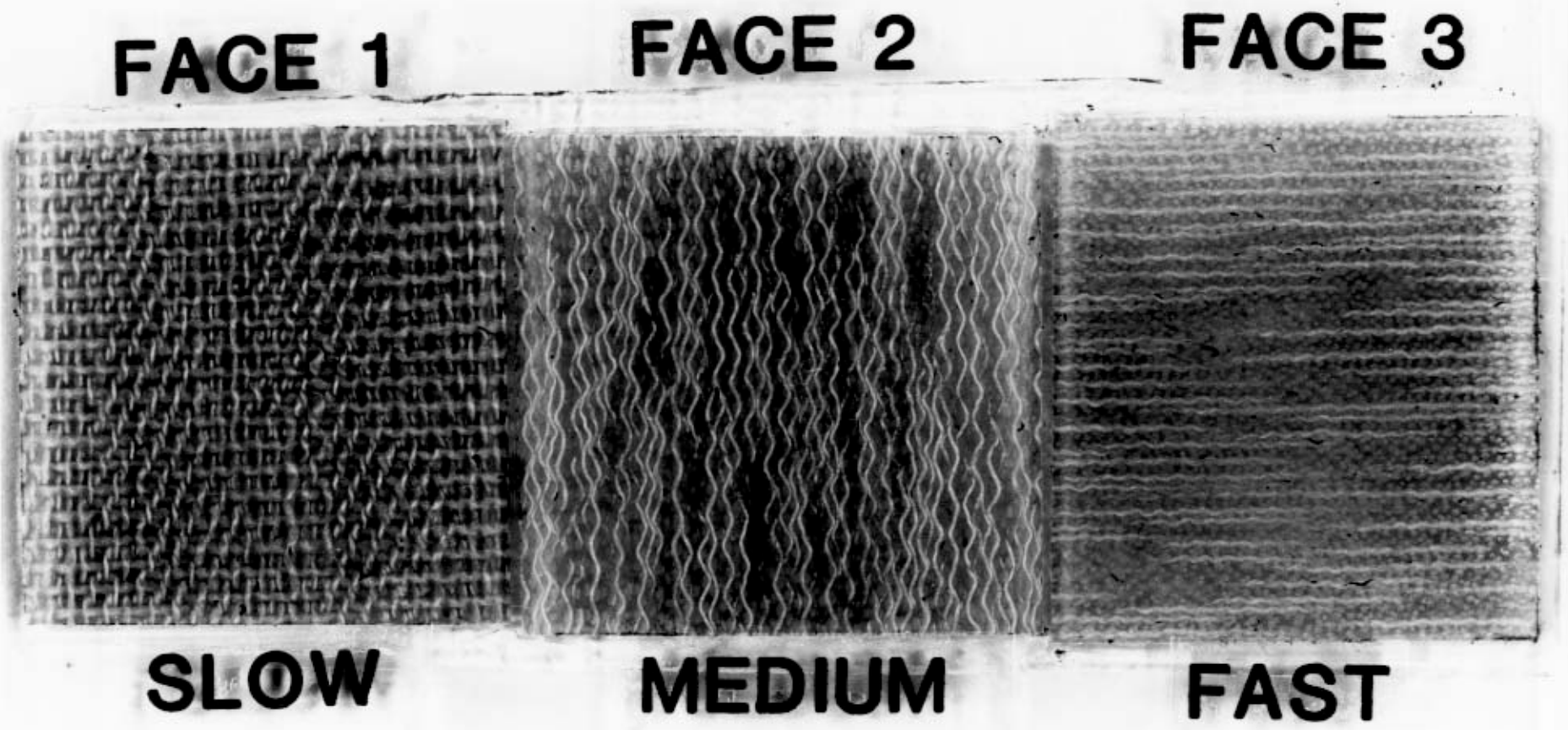

FIG. 9. Thin sections cut parallel to the three faces of a cube of the phenolic show the variation in canvas fibre densities assumed to be related to the measured anisotropic elastic properties.

shaly sequences, while azimuthal anisotropy is used to describe the idealized case of vertical aligned fractures. Both of these examples would be degenerate cases of the more general orthorhombic system. Two or more sources of anisotropy superimposed within the same lithologic unit, such as aligned vertical fracturing of a laminated sequence could result in orthorhombic anisotropy.

The conventional measure of anisotropy given by

$$\varepsilon = \left[Vp(90°) - Vp(0°)\right] / Vp(0°), \tag{18}$$

is not directly relevant to the case of multiple symetry axes. As Thomsen (1986, 1988) pointed out, this measure, at least in the cases of transverse isotropy and azimuthal anisotropy, is not always useful for either the computation of moveout velocities or the interpretation of Vs/Vp ratios for stress analysis. The term

$$\delta = 4\left[Vp(45°) / Vp(0°) - 1\right] - \left[Vp(90°) / Vp(0°) - 1\right] \tag{19}$$

was defined by Thomsen (1986) and used for moveout and stress analysis. Applying these measures to the velocity ratios measured in the directions used for this study produces values that fall within the range of the values reported by Thomsen (1986) for a variety of rocks. It is not yet clear if the moveout patterns observed on surface seismic gathers recorded with the phenolic can be conveniently modeled in the same manner described by Thomsen.

CONCLUSIONS

Ultrasonic modeling with Phenolic CE laminate has demonstrated the anisotropic elastic properties of the material. The patterns of shear-wave splitting observed on each face of a cube of the phenolic, along with the measured compressional velocities, were used to define orthogonal principal axes related to the slow, medium and fast directions through the material. Shear and compressional velocities were also measured in directions 45° to two of the principal axes and perpendicular to the other axis. Analysis of the data supports the interpretation of the anisotropy to be of orthorhombic symetry.

Physical modeling with the phenolic is currently being used to record shot gathers and simulated VSP and crosswell experiments to assess the effects of a known anisotropy for these geometries, and to provide comparative data for the testing of numerical modeling schemes. The initial application of conventional NMO-based velocity analysis on surface shot gathers produced stacking velocities that differed considerably from expected values in some instances. Surface seismic data will record the combined effects of all the

anisotropic layers through which the wavefield may have passed. Clearly, moveout velocity analysis and imaging for media with orthorhombic anisotropy represents a major challenge for multicomponent seismology.

REFERENCES

Aki, K. and Richards, P. G., 1980, Quantitative seismology: Theory and methods: W. H. Freeman and Co.

Banik, N. C., 1984, Velocity anisotropy of shales and depth estimation in the North Sea basin: Geophysics, 49, 1411-1419.

Brown, R. J., 1989, Relationships between the velocities and the elastic constsants of an anisotropic solid possessing orthorhombic symmetry.

Bullen, K.E., 1963, An introduction to the theory of of seismology: Cambridge University Press.

Crampin, S., 1981, A review of wave motion in anisotropic and cracked elastic-media: Wave Motion, 3, 343-391.

----------1984, An introduction to wave propagation in anisotropic media: Geophys. J. Roy. Astr. Soc., 49, 181-208.

---------- 1985, Evaluation of anisotropy by shear-wave splitting: Geophysics, 50, 142-152.

Fedorov, F.I., 1968, Theory of elastic waves in crystals: Plenum Press.

Helbig, K., 1983, Elliptical anisotropy - its significance and meaning: Geophysics, 48, 825-832.

Musgrave, M.J.P., 1970, Crystal acoustics: Holden-Day.

Nye, J.F., 1957, Physical properties of crystals: Oxford Press.

Thomsen, L., 1986, Weak elastic anisotropy: Geophysics, 51, 1954-1966.

---------- 1988, Reflection seismology over azimuthally anisotropic media: Geophysics, 53, 304-313.

Yale, D.P. and Sprunt, E.S., 1989, Prediction of fracture direction using shear acoustic anisotropy: The Log Analyst, March-April, p. 65-70.